

The two-point correlation function and morphological segregation in the *Optical Redshift Survey*

Sune Hermit,^{1,2} Basílio X. Santiago,² Ofer Lahav,² Michael A. Strauss,^{3,7}

Marc Davis,⁴ Alan Dressler⁵ and John P. Huchra⁶

¹ *Astronomical Observatory, Juliane Maries Vej 30, 2100 Kbh. Ø, Denmark*

² *Institute of Astronomy, Cambridge University, Madingley Road, Cambridge CB3 0HA, United Kingdom*

³ *Dept. of Astrophysical Sciences, Princeton University, Princeton, NJ 08544, U.S.A.*

⁴ *Physics and Astronomy Departments, University of California, Berkeley, CA 94720, U.S.A.*

⁵ *Observatories of the Carnegie Institution of Washington, 813 Santa Barbara Street, Pasadena CA 91101, U.S.A.*

⁶ *Center for Astrophysics, 60 Garden Street, Cambridge, MA 02138, U.S.A.*

⁷ *Alfred P. Sloan Foundation Fellow*

July 26, 1996

ABSTRACT

We study the clustering of galaxies in real and redshift space using the Optical Redshift Survey (ORS). We estimate the two point correlation function in redshift space, $\xi(s)$, for several subsamples of ORS, spanning nearly a factor of 30 in volume. We detect significant variations in $\xi(s)$ among the subsamples covering small volumes. For volumes $\gtrsim (75h^{-1}\text{Mpc})^3$, however, the ORS subsamples present very similar clustering patterns. Fits of the form $\xi(s) = (\frac{s}{s_0})^{-\gamma_s}$ give best-fit values in the range $1.5 \leq \gamma_s \leq 1.7$ and $6.5 \leq s_0 \leq 8.8h^{-1}\text{Mpc}$ for several samples extending to redshifts of 8000 km s^{-1} . However, in several cases $\xi(s)$ is not well described by a single power-law, rendering the best-fit values quite sensitive to the interval in s adopted. We find significant differences in clustering between the diameter-limited and magnitude-limited ORS samples within a radius of 4000 km s^{-1} centered on the Local Group; $\xi(s)$ is larger for the magnitude-limited sample than for diameter-limited one. We interpret this as an indirect result of the morphological segregation coupled with differences in morphological mix. We split ORS into different morphological subsamples and confirm the existence of morphological segregation of galaxies out to scales of $s \sim 10h^{-1}\text{Mpc}$. Our results indicate that the relative bias factor between early type galaxies and late-types may be weakly dependent on scale. If real, this would suggest non-linear biasing.

We also compute correlations as a function of radial and projected separations, $\xi(r_p, \pi)$, from which we derive the real space correlation function, $\xi(r)$. We obtain values $4.9 \leq r_0 \leq 7.3h^{-1}\text{Mpc}$ and $1.5 \leq \gamma_r \leq 1.7$ for various ORS samples. As before, these values depend strongly on the range in r adopted for the fit. The results obtained in real space confirm those found using $\xi(s)$, i.e. in small volumes, magnitude limited samples show larger clustering than do diameter limited ones. There is no difference when large volumes are considered. Our results prove to be robust to adoption of different estimators of $\xi(s)$ and to alternative methods to compensate for sampling selection effects.

Key words: methods: statistical; galaxies: clustering; cosmology: large-scale structure of Universe

1 INTRODUCTION

Early redshift surveys showed that galaxies are not distributed randomly in the Universe (Oort 1983). They are found to lie in clusters, filaments, bubbles and sheet-like structures (Davis et al. 1982, de Lapparent, Geller & Huchra 1986, Pellegrini et al. 1989). There exist large regions of the

Universe which are almost devoid of galaxies (Kirshner et al. 1981, Geller & Huchra 1988, de Lapparent, Geller & Huchra 1988). This wealth of information about galaxy clustering and general distribution properties provide constraints on theories of galaxy and large-scale structure formation (Peebles 1980, Dekel & Rees 1987, Strauss & Willick 1995).

To characterize the distribution of galaxies and to quantify the degree to which it departs from a Poisson distribution, a number of statistical tools have been developed. The first and most widely used approach to quantify the degree of clustering in a galaxy sample has been the two-point correlation function (Totsuji & Kihara 1969, Peebles 1980). In spite of its known limitations, it has been applied to all redshift surveys completed to date (e.g. Moore et al. 1994, Martínez & Coles (1994) [IRAS QDOT], Dalton et al. 1994 [APM Clusters], Loveday et al. 1995 [Stromlo-APM], de Lapparent et al. 1988, Park et al. 1994 [CfA2], Fisher et al. 1994 [IRAS 1.2 Jy]). Similarly, higher-order clustering properties have been studied by means of the three and four-point correlation functions or by using counts in cells statistics (e.g. Efstathiou, Sutherland & Maddox 1990, Bouchet et al. 1993). Recent efforts have also been invested into directly reconstructing the galaxy density field (Saunders et al. 1991, Scharf et al. 1992, Strauss et al. 1992, Hudson 1993, Fisher et al. 1995b) or studying its power-spectrum (Vogeley et al. 1992, Fisher et al. 1993, da Costa et al. 1994).

A limiting factor in comparing observed galaxy clustering properties with model predictions is the difficulty in assessing whether the observations reflect the properties of the ensemble of galaxies in the universe (de Lapparent et al. 1988). The search for a ‘fair sample’ of galaxies has led to the completion of ever larger redshift surveys, probing both depth and angular extent. A recent step towards this goal was the completion of the Optical Redshift Survey (ORS), covering 98% of the sky for $|b| \geq 20^\circ$ and containing about 8500 optically selected galaxies (Santiago et al. 1995, 1996). ORS is currently the closest approximation to an all-sky redshift survey selected in the optical and provides a dense sampling of the galaxy distribution out to 8000 km s^{-1} .

The particular selection criteria used to define a redshift sample may introduce systematic effects on the derived clustering properties of galaxies. Most samples are drawn from galaxy catalogues by applying either a diameter or a magnitude cut-off limit to them. Thus, it is important to establish if diameter-limited and magnitude-limited surveys sample the general galaxy population in a uniform way. In fact, comparisons between diameter and magnitude limited samples have been made by Zucca et al. (1991) but with much smaller samples. ORS is again an excellent dataset for such analyses, given that it is essentially complete in both diameters ($\theta > 1.9'$) and magnitudes ($m_B \leq 14.5$).

Finally, an important observational result of previous galaxy clustering analyses is the existence of segregation as a function of morphological type. It has been qualitatively known for decades that elliptical or bulge-dominated (‘early-type’) galaxies prevail in the cores of rich clusters of galaxies whereas disk-dominated galaxies (spirals) make up most of the general field population (Hubble & Humason 1931, Abell 1965). This result is often described as the so called morphology-density relation, first quantified by Dressler (1980) for clusters, and also known to apply for smaller galaxy concentrations such as groups (Postman & Geller 1984, Ferguson & Sandage 1991). A morphology-radius relation have also been suggested (Whitmore, Gilmore & Jones 1993). Indications that morphological segregation also exists among field galaxies have been given by several works (Davis & Geller 1976, Giovanelli, Haynes & Chincarini 1986, Eder et al. 1989, Lahav, Nemiroff & Piran 1990, Mo &

Börner 1990, Santiago & Strauss 1992). While morphological segregation is fairly well established, at least on scales up to $\sim 10h^{-1} \text{ Mpc}$ ($H_0 = 100h \text{ km s}^{-1} \text{ Mpc}^{-1}$), it has been more difficult to establish if the clustering properties of galaxies depend on luminosity (Phillipps & Shanks 1987, Alimi, Valls-Gabaud & Blanchard 1988, Davis et al. 1988, Hamilton 1988, Salzer, Hanson & Gavazzi 1990, Iovino et al. 1993, Park et al. 1994), surface brightness (Davis & Djorgovski 1985, Santiago & da Costa 1990, Thuan et al. 1991), spectral properties (Salzer et al. 1988) or circular velocity (White, Tully & Davis 1988, Mo & Lahav 1993). On the theoretical side, the existence of segregation among galaxies and the indirect evidence for segregation between light and matter on galactic and extra-galactic scales has led to the formulation of scenarios of biased galaxy formation (Kaiser 1984, Babul & White 1991).

In this paper we address the issues of clustering dependence on survey volume, sample selection criteria and morphology. The paper is structured as follows. In section 2 we briefly introduce the ORS data. In section 3 the different estimators of the two-point correlation function and their associated errors are presented. We also discuss different schemes to compensate for selection effects inherent to the data. In section 4 we present results based on the comparison of the correlation functions in redshift space, $\xi(s)$, for different ORS subsamples split according to volume, selection criteria and morphological types. In section 5 we compute $\xi(r_p, \pi)$, the correlation as a function of radial and projected separations, and invert it to obtain the real-space correlation, $\xi(r)$. Our results for $\xi(r)$ are consistent with those of section 4. Finally, in section 6 we state our main conclusions and discuss our results.

2 THE DATA

ORS was presented by Santiago et al. 1995 (hereafter Paper I). In brief, the sample was drawn from three catalogues: the Uppsala General Catalogue of Galaxies (UGC; Nilson 1973), the European Southern Observatory Galaxy Catalogue (ESO; Lauberts 1982, Lauberts & Valentijn 1989) and the Extension to the Southern Galaxy Catalogue (ESGC; Corwin & Skiff 1994). ORS contains two largely overlapping subsamples, one magnitude limited to $m_B \leq 14.5$ (hereafter ORSm) and the other diameter limited to $\theta_B \geq 1.9'$ (hereafter ORSd). ORSd was created by merging ESGC, ESOD and UGCd, and ORSm consists of ESOM and UGCm. The entire ORS catalog consists of 8457 objects; redshifts are available for 8266. To complete the sample, roughly 1300 new redshifts were measured – the remaining redshifts were taken from the literature. Most of the new redshifts were obtained in regions of low galactic latitude, $20^\circ \leq |b| \leq 30^\circ$, and within the strip not covered by either the UGC or ESO catalogues ($-17.5 \leq \delta \leq -2.5$). ORS provides the most detailed and homogeneous sampling to date of these areas of the sky. The matching of the catalogs and the derivation of the luminosity and diameter functions for the ORS are treated in Santiago et al. (1996) (hereafter Paper II).

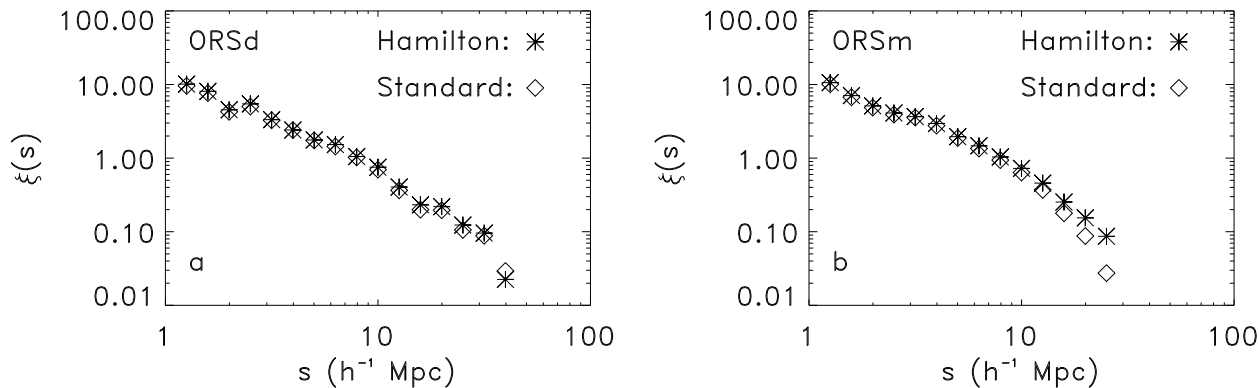


Figure 1. The correlation function for ORSd (panel a) and ORSm (panel b) out to $V_{max} = 8000 \text{ km s}^{-1}$ using the Hamilton (stars) and Standard estimator (diamonds).

3 THE TWO-POINT CORRELATION FUNCTION

Consider a Poissonian distribution of points in space. The joint probability that one point is found in each of two independent volume elements dV_1 and dV_2 obviously scales with the mean density and the size of the volume elements

$$dP = \bar{n}^2 dV_1 dV_2. \quad (1)$$

If the distribution is non-Poissonian then there may be an excess probability of finding a point in each of the two volume elements dV_1 and dV_2 separated by the distance r (see, e.g. Peebles 1980):

$$dP = \bar{n}^2 dV_1 dV_2 [1 + \xi(r)]. \quad (2)$$

This excess probability, quantified by $\xi(r)$, is the two-point correlation function.

Traditionally, $\xi(r)$ has been determined by the expression

$$\xi_S(r) = \frac{\bar{n}_R}{\bar{n}_D} \frac{DD(r)}{DR(r)} - 1, \quad (3)$$

where $DD(r)$ and $DR(r)$ are, respectively, the number of galaxy-galaxy and galaxy-random pairs with separation within the range r and $r + dr$. The latter are computed by creating a catalogue of randomly distributed points within the same volume occupied by the real galaxies. \bar{n}_D (\bar{n}_R) is the number density of galaxies (random points) in this volume. We hereafter refer to $\xi_S(r)$ as the standard estimator. In spite of its widespread usage, the standard estimator explicitly depends on the mean density assigned to the sample. As the lack of a fair sample may bias \bar{n}_D , $\xi_S(r)$ may be (under) overestimated accordingly (de Lapparent et al. 1988, Davis et al. 1988). More recently, Hamilton (1993) has proposed an alternative estimator, which is much less sensitive to this problem:

$$\xi_H(r) = \frac{DD(r)RR(r)}{[DR(r)]^2} - 1, \quad (4)$$

where $RR(r)$ is the random-random pair counts within the bin of separation r . Hamilton (1993) shows that the dependence of $\xi_H(r)$ on the mean density of galaxies in the survey volume is of second order, whereas the dependence of $\xi_S(r)$

is of first order. Thus $\xi_H(r)$ is less affected by the uncertainty in the mean density.

In Fig. 1, we compare the two estimators in redshift space, $\xi_H(s)$ and $\xi_S(s)$, for both ORSd and ORSm cut at $V_{max} = 8000 \text{ km s}^{-1}$. Throughout this paper, we adopt the usual convention and use $\xi(s)$ ($\xi(r)$) to denote the correlation function in redshift (real) space. The two estimators give very similar results in both cases except on the largest scales, where the clustering is weak. A similar trend was found by Loveday et al. (1995), who analysed the Stromlo-APM survey. Since $\xi_H(s)$ gives a more reliable estimate of the two-point correlation function on all scales, we chose to use that estimator exclusively in what follows.

In practice, the pair counts DD , DR and RR are weighted sums of pairs, which take into account the selection effects inherent to the galaxy sample used (see §3.1 below). Likewise for the mean number density \bar{n}_D . The catalogue of random points may or may not imitate such selection effects, provided that the appropriate selection function is applied to compensate for them. In this paper we did not introduce any selection effects to the random points. The weighting scheme adopted in this work is the topic of the next subsection.

3.1 Weights and selection functions

In a diameter or magnitude limited survey, the sample will become sparser at larger redshifts due to the increasing loss of galaxies caused by the adopted apparent magnitude or diameter cut-off. This selection effect has to be correctly accounted for when determining $\xi(s)$ or any other statistic from the sample. The effect is quantified by the selection function, $\phi(\mathbf{r})$, which expresses the fraction of the total population of galaxies that are expected to satisfy the sample's selection criterion at any given point in space. Under the assumption of a universal luminosity (or diameter) function, the selection function depends solely on distance. For ORS, however, an angular dependence is introduced by variable (and non-negligible) amounts of Galactic extinction as well as by non-uniformities in the magnitude or diameter systems among the three different catalogues from which the data were derived. Paper II presents a detailed discussion of

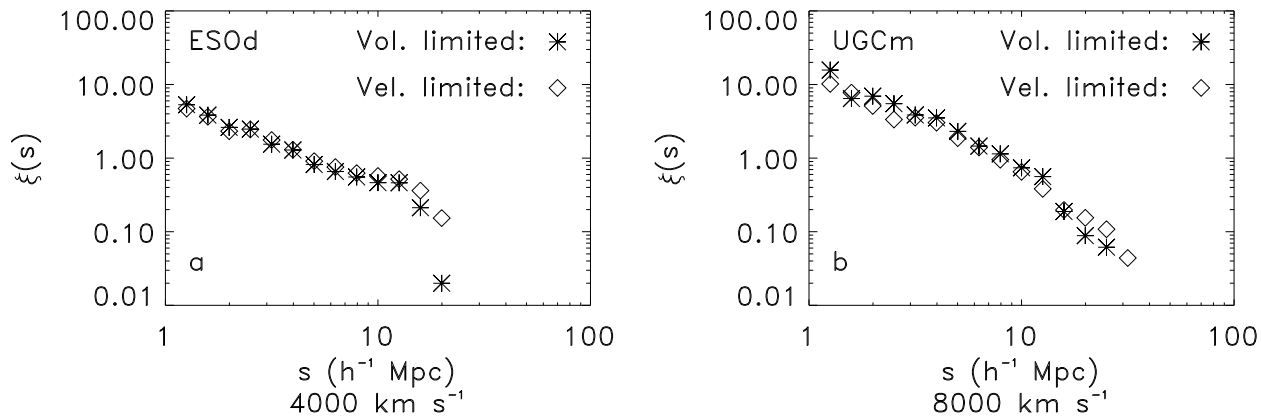


Figure 2. Comparison of volume (stars) and velocity (diamonds) limited subsamples for ESOd (panel a) and UGCm (panel b).

the problem and of the way these additional selection effects were incorporated into $\phi(\mathbf{r})$. In brief, extinction effects were incorporated into the maximum likelihood approach used to fit $\phi(\mathbf{r})$ (see also Yahil et al. 1991). A selection function was also fitted separately to each of the five ORS subsamples (ESOm, ESOd, UGCm, UGCd and ESGC) in order to bypass the inhomogeneity in selection caused by the different catalogues.

Once $\phi(\mathbf{r})$ is available, selection effects are in principle compensated for by weighting each galaxy i by $w_i = 1/\phi(\mathbf{r}_i)$. However, the different subsamples in ORS have different diameter and/or magnitude systems, which introduces an additional selection bias: subsamples based on deeper plate material tend to contain more galaxies and thus have a larger mean number density (Paper II). We thus normalize each subsample by the mean number density of galaxies in that subsample. This would be adequate if each subsample in itself were a fair sample, but that it not necessarily the case, and thus, as explained in Paper II, we renormalize again by the mean density of each subsample volume relative to the full sky, as found in the full-sky *IRAS* 1.2 Jy sample (Fisher et al. 1995a). We thus assign galaxy i a weight given by

$$w_i = \frac{1}{\phi(\mathbf{r}_i) n_{k,ORS}} \frac{n_{k,IRAS}}{n_{tot,IRAS}}, \quad (5)$$

where $n_{k,ORS}$ ($n_{k,IRAS}$) is the mean number density in the region corresponding to the k^{th} subsample in ORS (*IRAS*) and $n_{tot,IRAS}$ is the total mean number density as computed from the *IRAS* 1.2 Jy sample. All number densities correspond to a volume-limiting distance of 500 km s^{-1} (cf., Paper II).

The weighting scheme used here is not minimum variance, in the sense of Davis & Huchra (1982) and Efstathiou (1988). However, minimum weighting requires prior knowledge of the correlation function. This problem has been bypassed in the past by usage of earlier estimates of $\xi(r)$ or of N-body simulations (Loveday et al. 1992,1995). For a dense sample like ORS, however, the practical improvement provided by using a minimum variance method is very small (Hamilton 1993, Park et al. 1994).

Finally, we should point out that the results presented in the next sections have been tested with different weighting schemes and prove to be robust.

3.2 Error estimation

There is no standard method of calculating errors for correlation functions (Hamilton 1993, Strauss & Willick 1995). One could simply assume Poisson fluctuations in the pair counts, but since they are correlated on any given scale, this is not strictly correct. Instead we use 10 bootstrap resamplings of the data (Barrow, Bhavsar & Sonoda 1984, Ling, Frenk & Barrow 1986, Mo, Jing & Börner 1992) to estimate the variance in the calculated correlation functions. As shown by Fisher et al. (1994), this is likely to be an overestimate of the real errors and is thus appropriate given the conservative approach we adopt throughout this paper.

4 CLUSTERING IN ORS

The ORS subsamples used here are limited at $V_{max} = 8000 \text{ km s}^{-1}$ in order to minimize shot noise. The selection function parameters for those subsamples with $V_{max} = 8000 \text{ km s}^{-1}$ are listed in Table 1 of Paper II. As mentioned before, to calculate $\xi(s)$ we created random samples with the same geometry as the data sample in consideration; in the case of ORSd, for example, we limited the random sample to 8000 km s^{-1} , $|b| \geq 20^\circ$ and to regions with $A_B \leq 0.7$ as determined from the extinction maps of Burstein & Heiles (1982). When dealing with ESOm (and therefore ORSm) we also took into account the lack of ESO-LV magnitudes in several ESO plates and thus did not place random points within the boundaries of these plates (see Paper I for details).

We assigned unit weight to the random points and used logarithmic binning on all scales. We tested the code and our random number generator by computing $\xi(s)$ on several pairs of random samples consisting of 20000 points each. As expected, this yielded no correlations on scales $s \geq 0.5h^{-1} \text{ Mpc}$. As a final test of our code, we calculated $\xi(s)$ for the *IRAS* 1.2 Jy sample (Fisher et al. 1995a) and successfully recovered the results of Fisher et al. (1994).

An important issue is to test the reliability of the weights assigned to each galaxy. We do that by comparing subsamples cut at a given maximum distance V_{max} (hereafter referred to as velocity-limited at V_{max}) to their volume-

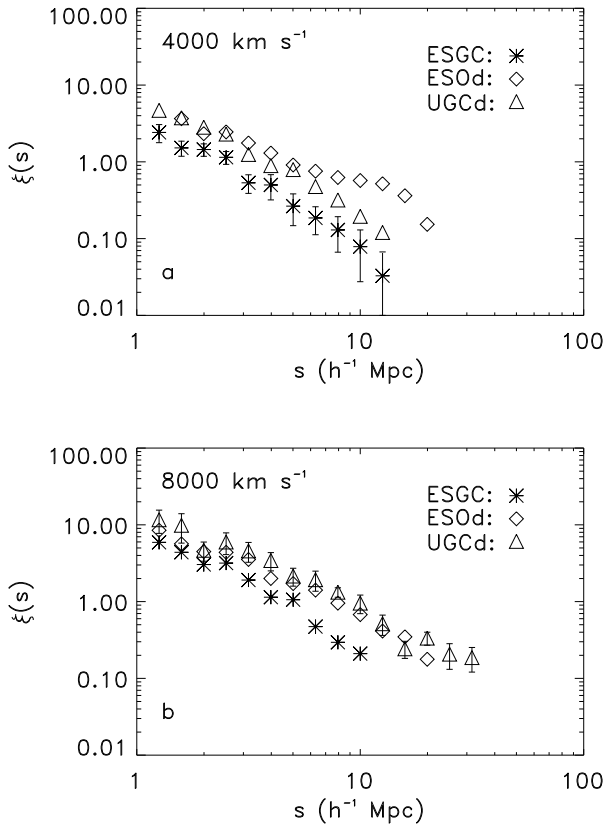


Figure 3. Panel a: $\xi(s)$ for ESGC (stars), ESOD (diamonds) and UGCd (triangles) cut at $V_{max} = 4000 \text{ km s}^{-1}$. Panel b: The same, but for subsamples cut at $V_{max} = 8000 \text{ km s}^{-1}$.

limited counterparts. These latter subsamples, by definition, include only objects which are luminous (or large) enough to satisfy the selection criteria of the survey if they were at V_{max} . This is equivalent to applying a lower limit to the luminosity (or absolute diameter) to the subsample, leading to a uniformly selected dataset with unit weight assigned to each object ($\phi(r) = 1, 0 \leq r \leq V_{max}$). Since both velocity and volume-limited subsamples probe the same volume in space, they should lead to very similar $\xi(s)$, unless the weights in the velocity-limited subsample are biased or there is segregation as a function of luminosity (or absolute diameter). The results are plotted in Fig. 2. Panel *a* shows ESOD out to $V_{max} = 4000 \text{ km s}^{-1}$ and panel *b* refers to UGCm out to $V_{max} = 8000 \text{ km s}^{-1}$. The agreement is very good in both panels, especially when one considers the relatively small number of galaxies in the volume limited samples (386 and 433 objects in panels *a* and *b*, respectively). We are therefore confident that the selection function derived in Paper II is reliable and hereafter continue working with velocity-limited subsamples.

Finally, we note that redshifts are a combination of the Hubble flow and peculiar velocities, the latter distorting the determination of galaxy clustering in redshift space. In the remainder of this section we present correlation functions for ORS in redshift space, $\xi(s)$. Since the main purpose of this work is to compare $\xi(s)$ for different samples, we adopt the working hypothesis that, to first order, peculiar velocities

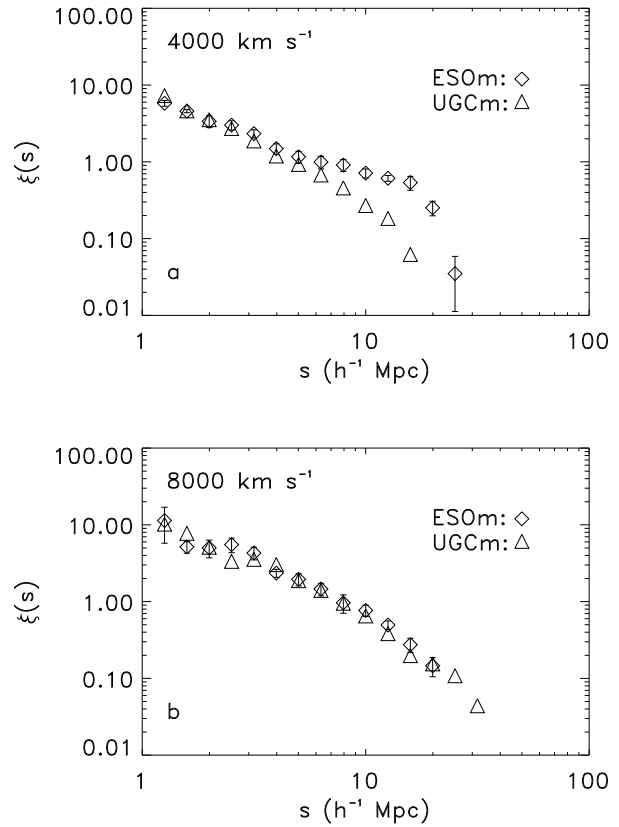


Figure 4. The same as Fig. 3 but for magnitude limited subsamples.

will affect the samples being compared in similar ways. In section 5 we calculate the real-space correlation function, and find similar results to those in this section, confirming our working hypothesis.

4.1 $\xi(s)$ for the different subsamples

If a survey sampling the local universe contains structures whose sizes are comparable to the volume of the survey itself, it is not considered a ‘fair sample’ of the large-scale galaxy distribution. A detailed discussion of the effect of such survey-sized structures is presented by de Lapparent et al. (1988). Therefore, it is important to define the minimum survey volume which would satisfy the condition for being a fair sample. Since ORS provides us with a dense sampling of the local universe over two-thirds of the celestial sphere, we here investigate whether it may be considered a fair sample, at least for the purpose of estimating $\xi(s)$. We thus compute $\xi(s)$ separately for the 5 ORS subsamples (ESOD, UGCd, ESGC, ESOM and UGCm) both out to $V_{max} = 4000 \text{ km s}^{-1}$ and $V_{max} = 8000 \text{ km s}^{-1}$, with volumes spanning nearly a factor of 30.

The results for the diameter-limited data are plotted in Fig. 3 and the corresponding plots for the magnitude limited subsamples are in Fig. 4. Errorbars denote one standard deviation from the distribution of $\xi(s)$ for the 10 bootstrap resamplings mentioned in section 3.2. For clarity, we have

only plotted errors for one of the subsamples in each of the two panels in Fig. 3 and Fig. 4. In panel 3a we plot errors for ESGC. It is the smallest of the ORS subsamples and correspondingly the one that has largest associated errors.

The differences in $\xi(s)$ are significant for the subsamples shown in panels 3a and 4a. There are large discrepancies between UGC and ESO on scales $7 - 20h^{-1}$ Mpc regardless of selection criteria. ESGC seems to exhibit a slightly steeper slope and a much smaller correlation length than both the ESOd and UGCd samples. For $V_{max} = 8000 \text{ km s}^{-1}$, however, $\xi(s)$ is very similar for the ESO and UGC subsamples. This is true in both figures 3 and 4. The ESGC $\xi(s)$ still has a smaller amplitude at $V_{max} = 8000 \text{ km s}^{-1}$ than do ESOd and UGCd. ESGC, however, covers a volume less than half of that of ESOd and less than a third of UGCd. We thus conclude that the ESOd and UGCd subsamples stretching out to $V_{max} = 8000 \text{ km s}^{-1}$ are close approximations to a fair sample (at least for the purpose of estimating $\xi(s)$ within $20h^{-1}$ Mpc), whereas ESGC and the subsamples limited at $V_{max} = 4000 \text{ km s}^{-1}$ are not. The minimum volume that supposedly contains a representative sample of the ensemble, for these purposes, is thus $\sim (75h^{-1}\text{Mpc})^3$. Notice that in both ESO and UGC, diameter and magnitude-limited subsamples have a similar $\xi(s)$ slope. The latter, however, are more clustered for $V_{max} = 4000 \text{ km s}^{-1}$ but not for $V_{max} = 8000 \text{ km s}^{-1}$. This issue will be revisited in §4.2.

For each of the subsamples large enough to be considered good approximations to a fair sample we fit a power-law of the form

$$\xi(s) = \left(\frac{s}{s_0}\right)^{-\gamma_s} \quad (6)$$

and determine the best-fit value of the slope γ_s and correlation length s_0 using a least squares fit. The scale ranges used in the fits and the derived values are listed in Table 1. The best-fit values span the range $1.5 \leq \gamma_s \leq 1.7$ and $6.5 \leq s_0 \leq 8.8h^{-1}$ Mpc. However, some of the cases shown in Fig. 3 and Fig. 4 are not well described by a single power-law over all scales. The presence of curvature in $\xi(s)$ is also visible in the APM (Loveday et al. 1995) and quite pronounced in the QDOT sample (Moore et al. 1994). Moore et al. (1994) hypothesize that this is caused by a combination of peculiar velocities and observational errors which will enhance the correlations on small scales and suppress them on larger scales. Since the $\xi(s)$ are not perfect power-laws, the values listed in Table 1 are very sensitive to the scale interval used in the fits. For instance, if we fit a power-law to $\xi(s)$ for ORSd (ORSm) limited at $V_{max} = 8000 \text{ km s}^{-1}$ over the range $1 \leq s \leq 10h^{-1}$ Mpc, we find $s_0 = 8.19(8.58)$ and $\gamma_s = -1.26(-1.18)$. If the fitted range is $3 \leq s \leq 16h^{-1}$ Mpc, however, the results are $s_0 = 7.36(7.65)$ and $\gamma_s = -1.58(-1.62)$. The ranges listed in Table 1 are thus the ones where $\xi(s)$ was best fit by a single power-law. Also, due to the fact that the points are not statistically independent, it is not strictly correct to use a least square method for this purpose. However, as demonstrated by Bouchet et al. (1993), it is a good first approximation, and in any case the uncertainty in the fitted values will be dominated by the strong dependence on the range in s chosen for the fit.

We now compare our $\xi(s)$ determinations with those of

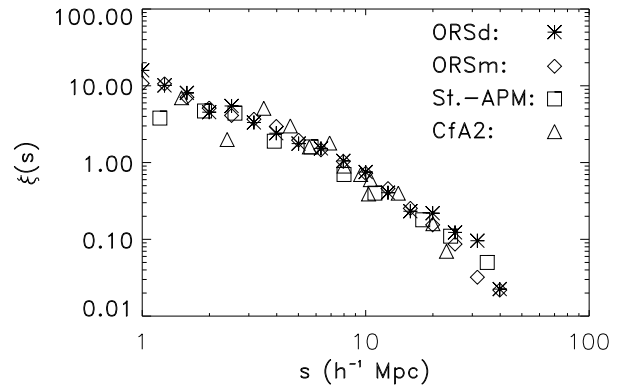


Figure 5. Comparison of $\xi(s)$ for ORSd (stars) and ORSm (diamonds) out to $V_{max} = 8000 \text{ km s}^{-1}$ with previous estimates based on optical samples: Stromlo-APM (squares) and CfA2 (triangles).

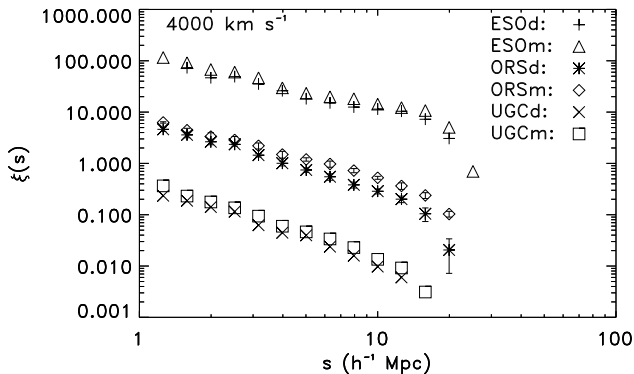
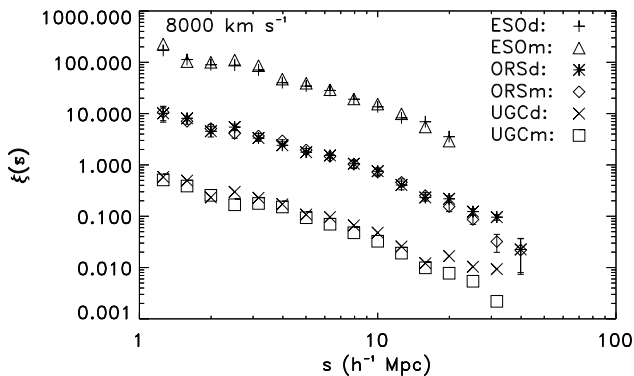
other authors. We use the ORSd and ORSm correlations for that purpose. Power-law fits to these latter are listed in the last two lines of Table 1. Our $\xi(s)$ for ORSd and ORSm are in excellent agreement with the results obtained by de Lapparent et al. (1988) and by Loveday et al. (1995) for the CfA2 and Stromlo-APM samples, respectively, as shown in Fig 5. These previous works probe larger volumes than does ORS but contain a smaller number of galaxies, hence our smoother $\xi(s)$. Notice that the best-fit values to Eq. (5) quoted by Loveday et al. (1995) are significantly different from those listed in Table 1. This is entirely due to differences in the scale range used in the fits, which illustrates the sensitivity of the fitted values on the interval in s used. Finally, our ORSd and ORSm $\xi(s)$ are also in excellent agreement with those determined by Davis & Peebles (1983) and Maurogordato, Schaeffer & da Costa (1992) for the CfA1 and SSRS samples, respectively. This is not very surprising given the fact that the UGCm and CfA1 overlap considerably, as do ESOd and SSRS.

4.2 ORSd and ORSm

The correlation function $\xi(s)$ for both ORSd and ORSm samples can be seen in Fig. 6 and Fig. 7 for $V_{max} = 4000 \text{ km s}^{-1}$ and $V_{max} = 8000 \text{ km s}^{-1}$, respectively. Also shown are the equivalent correlations for ESO and UGC subsamples. These latter have been offset by a constant for clarity. The errorbars again indicate 1σ deviations as determined from the 10 bootstrap resamplings. The ORSd and ORSm samples within $V_{max} = 4000 \text{ km s}^{-1}$ have significantly different correlation functions. ORSm is more clustered than ORSd over the entire range of scales available. Similar behaviour is seen for both ESO and UGC; the magnitude limited subsamples are more clustered than their diameter-limited counterparts in Fig. 6. Thus, it appears that the difference in clustering amplitude between ORSd and ORSm arises from similar contributions from the ESO and UGC subsamples. On the other hand, for $V_{max} = 8000 \text{ km s}^{-1}$, the ORSd and ORSm have very similar $\xi(s)$, except on the very largest scales, where ORSm falls off faster than ORSd (Fig. 7).

Table 1. Power-law fits and parameters

Sample	Limit (h^{-1} Mpc)	Range (h^{-1} Mpc)	γ_s	s_0	γ_r	r_0
ESOd	80	2.5 - 20	1.48	7.2	-	-
ESOm	80	2.5 - 20	1.65	7.5	-	-
UGCd	80	2.5 - 32	1.48	8.8	-	-
UGCm	80	1.6 - 32	1.64	6.5	-	-
ORSd	80	1 - 40	1.57	6.6	1.59	7.07
ORSm	80	1.3 - 25	1.51	6.8	1.56	7.26

**Figure 6.** The correlation function for ORSd (stars) and ORSm (diamonds) velocity limited at 4000 km s^{-1} . For comparison we also show $\xi(s)$ for ESOd (plus signs), ESOm (triangles), UGCd (crosses) and UGCm (squares). These latter are offset by a factor of 20 for the sake of clarity.**Figure 7.** The same as Fig. 6, only for samples velocity limited at 8000 km s^{-1} .

The only substantial difference between the ORSm and ORSd volumes is the ESGC strip ($-17.5^\circ < \delta < -2.5^\circ$), which is not included in ORSm. Thus it is unlikely that the difference in the ORSm and ORSd correlations to 4000 km s^{-1} is due to large-scale differences in the underlying density field. To make sure, we removed ESGC from ORSd and computed $\xi(s)$ again. Fig. 6 remained essentially unchanged; the vast majority of DD, DR and RR pairs in fact come from within ESOd, UGCd or from ESOd/UGCd cross-boundary pairs.

The observed discrepancy between ORSm and ORSd in

Figure 8. The frequency of morphological type for ORSd (dashed lines) and ORSm (solid lines) at $V_{max} = 4000 \text{ km s}^{-1}$ (panel a) and $4000 < V_{max} < 8000 \text{ km s}^{-1}$ (panel b). The difference in morphological mix is clearly diminished at larger redshifts, rendering more similar results for $\xi(s)$.

Fig. 6 is likely to reflect real clustering differences between magnitude-limited and diameter-limited samples. Since the former tend to pick up, on average, higher surface brightness, earlier type galaxies than the latter, one expects ORSm to show enhanced clustering as a result of the larger fraction of stronger clustered early-type galaxies it contains. The distributions of morphological types in ORSd (dashed lines) and ORSm (solid lines) are shown in Fig. 8 for $V_{max} = 4000 \text{ km s}^{-1}$ (panel a) and $4000 < V_{max} < 8000 \text{ km s}^{-1}$ (panel b). As expected, the morphological composition of ORSm is clearly skewed towards early-types relative to ORSd. Thus, the larger clustering in ORSm seen in Fig. 6 reflects segregation as a function of morphology and/or surface brightness. As attested by panel 8 b, the fraction of late-type, low surface brightness galaxies in ORSm and ORSd is markedly reduced beyond $V \sim 4000 \text{ km s}^{-1}$. This is expected to occur in any flux-limited (or diameter-limited) sample since these galaxies tend also to be less luminous (and smaller) than typical spirals and ellipticals. The reduced difference in the morphological mix of ORSm and ORSd for $V_{max} = 8000 \text{ km s}^{-1}$ renders their $\xi(s)$ very similar in this larger volume.

Since morphological segregation is more pronounced in

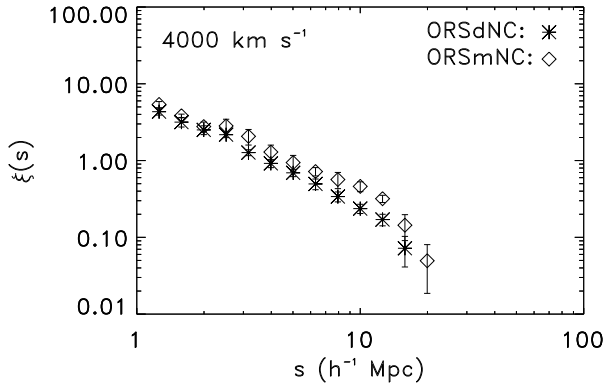


Figure 9. The correlation function for the cluster-removed ORSd and ORSm samples velocity limited at $V_{max} = 4000 \text{ km s}^{-1}$.

clusters, we test the effect described above by removing the 6 clusters shown in Table 2 and rederiving $\xi(s)$ for both ORSm and ORSd out to $V_{max} = 4000 \text{ km s}^{-1}$. This list contains the most prominent clusters within this volume. Columns 1, 2, 3 and 4 list the name and position of each cluster. Columns 5 and 6 give the length of the finger-of-God and the angular radius assumed to be covered by the cluster on the sky. Columns 7 and 8 give the number of galaxies in each cluster for ORSm and ORSd. Figure 9 show the result of this experiment. The difference in $\xi(s)$ is now clearly reduced (notice the change in the range in $\xi(s)$ relative to Fig. 6). We thus confirm that $\xi(s)$ depends on selection criteria as long as small and local volumes, containing a significant fraction of low surface brightness/late-types, are considered. The presence of high-density regions such as clusters may also enhance the dependence on selection criteria. This issue had already been addressed by Zucca et al. (1991), who found very similar correlation functions for magnitude and diameter-limited samples in the northern hemisphere, independent of the value used for V_{max} . Their result, however, was based on volume-limited samples containing at most 450 galaxies. In addition, the difference in morphological mix between their magnitude and diameter-limited samples limited at $V_{max} = 4000 \text{ km s}^{-1}$ is smaller than in ORSm and ORSd (see Table 3 of this paper and Table 2 of Zucca et al. 1991).

4.3 Morphological subsamples

In this section we investigate the existence of morphological segregation in ORS. We split each of the five ORS subsamples compared in section 4.1 into three morphologically selected subsamples: early-types ($T \leq 0$), Sab ($1 \leq T \leq 4$) and late-types ($T \geq 5$). The number of galaxies in each morphological bin for each ORS subsample is given in Table 3. We separately fit a selection function to each of these 15 morphological subsamples using the method described in Paper II and then merge the morphological subsamples together to create the corresponding ORSd and ORSm morphological subsamples. We are then left with 6 morphological subsamples, 3 for ORSm and 3 for ORSd.

We thus properly account for the selection effects in-

Table 3. Morphological Subsamples Limited at 4000 km s^{-1}

Sample	ESGC	ESOd	ESOm	UGCd	UGCm
Early	141	267	475	223	470
Sab	142	336	426	353	470
Late	317	542	404	681	617

Table 4. Power-law fits and parameters for the morphological subsamples

Sample	Type	limit ($h^{-1} \text{ Mpc}$)	Range ($h^{-1} \text{ Mpc}$)	γ_s	s_0
ORSd	Early	40	1.3 - 16	1.57	5.65
	Sab	40	1.3 - 16	1.53	4.24
	Late	40	1.3 - 16	1.35	3.78
ORSm	Early	40	1.3 - 16	1.52	6.70
	Sab	40	1.3 - 16	1.32	5.63
	Late	40	1.3 - 16	1.17	4.71

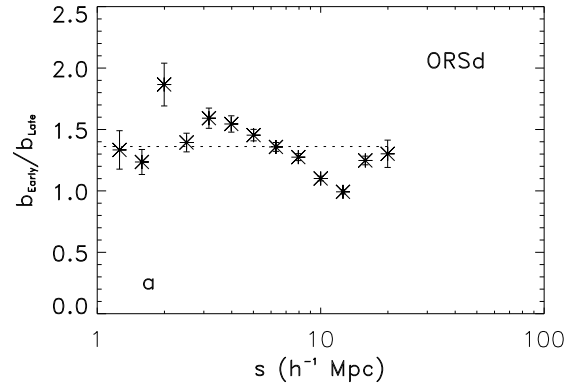
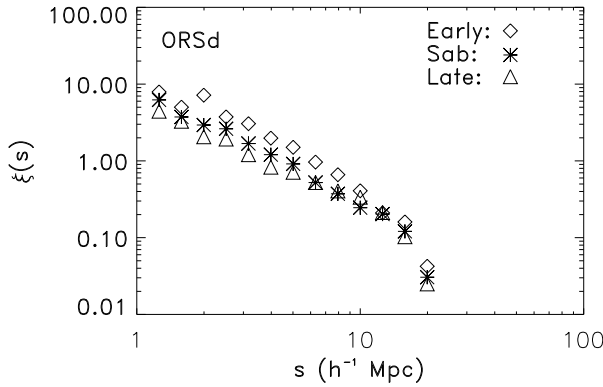
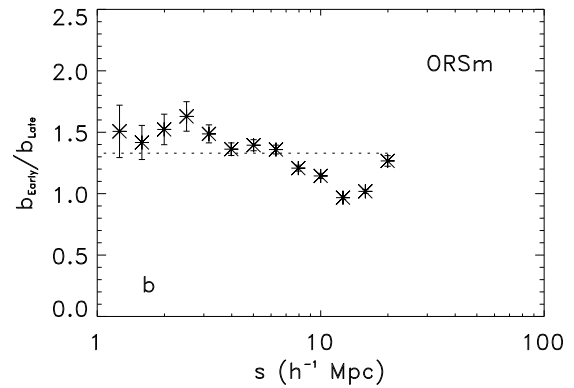
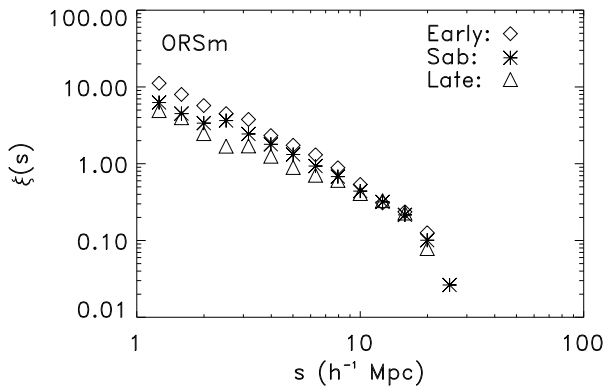
duced by the dependence of the luminosity (or diameter) function on morphology and by non-homogeneities in sample selection. In fact, the luminosity function is known to vary within the morphological bins defined above (Binggeli, Sandage & Tammann 1988, Loveday et al. 1992, Paper II). The broad morphological binning chosen in this work reflects the compromise between this dependence and the need to use sizeable samples to reliably derive $\phi(\mathbf{r})$ and $\xi(s)$. It also has the advantage of yielding subsamples with roughly similar numbers of objects and avoiding systematic differences in morphological classification likely to exist among the ESO, UGC and ESGC. In fact, it has been suggested that spirals may have been misclassified as early-types in UGC due to the lower quality plate material used for this catalog (Santiago & Strauss 1992). This effect is likely to be more pronounced at higher redshifts, and in fact some evidence of this is visible in the type-dependent selection functions used here.

Given the increasing sparseness of late-type galaxies ($T \geq 5$) beyond $V_{max} = 4000 \text{ km s}^{-1}$, leading to strong shot-noise problems, we decided to restrict our morphology-clustering investigation to $V_{max} = 4000 \text{ km s}^{-1}$. Thus, for each of the six morphological ORS subsamples we computed $\xi(s)$ using the samples limited at $V_{max} = 4000 \text{ km s}^{-1}$. The weighting is again given by the inverse of the new type-dependent selection functions, with the appropriate additional factors used when combining the ORS subsamples. The type correlation functions of ORSd and ORSm are shown in Fig. 10 and 11, respectively. Results from power-law fits are presented in Table 4. In each case the range in scales used was that where $\xi(s)$ was well approximated by a power-law.

From the figures and Table 4, we conclude that there is strong evidence for morphological segregation out to scales of $10h^{-1} \text{ Mpc}$ in both ORSd and ORSm. We thus confirm the results of many previous works, e.g., Lahav & Saslaw (1992), Santiago & Strauss (1992), Mo et al. (1992) and Loveday et al. (1995). The early-type galaxies are more clustered than the Sa/Sb galaxies, which in turn are more clustered than the late-type galaxies. For any given morpho-

Table 2. Parameters for removed clusters

Name	RA	DEC	V_{mean} (km s^{-1})	V_F (km s^{-1})	radius (deg.)	ORSm	ORSd
Hydra	158.625	-27.267	3450	1000	3.0	40	29
Centaurus	191.525	-41.033	3300	1000	6.0	75	43
Eridanus	51.500	-20.917	1590	400	3.0	20	15
Fornax	53.250	-35.500	1350	400	3.0	30	19
Ursa Major	178.625	+49.550	1020	300	6.0	37	39
Virgo	187.075	+12.667	1080	1500	6.0	148	109

**Figure 10.** Correlation functions for three morphologically selected subsamples of ORSd. Early types: diamonds, Spirals: stars, Late types: triangles.**Figure 12.** The relative biasing between early and late type galaxies in the ORSd (panel a) and ORSm (panel b). The dotted line is the mean value of b_{Early}/b_{Late} in each case.**Figure 11.** Same as Fig. 10, but for the ORSm.

logical subsample, $\xi(s)$ is very similar in both ORSd and ORSm.

By comparing the clustering amplitudes of different morphological subsamples we can infer the corresponding relative bias factor as a function of scale using the relation $\xi(s)_{Early} = b^2 \xi(s)_{Late}$. The scale dependence of b_{Early}/b_{Late} is shown in Fig. 12 for ORSd and ORSm. In spite of the noise in both panels of the figure, the two samples lead to quite similar results: $b_{Early}/b_{Late} \sim 1.5$ on small scales ($s \lesssim 3h^{-1}$ Mpc), with a declining trend towards larger scales, where $b_{Early}/b_{Late} \sim 1$. Relative bias factors can also be inferred from the fits made by Loveday et al. (1995) to their type-

dependent $\xi(s)$. A relative bias of $\sim 1.4 - 1.5$ between E/S0 and Spi/Irr is derived from their data at $s \sim 5h^{-1}$ Mpc. Removing the clusters listed in Table 2 makes little difference to the results. A scale dependence is also suggested by the UGC and ESO subsamples considered individually, indicating that it is not an artifact of the way we combined the subsamples or of the weighting scheme used. Such a scale dependence is expected from non-linear biasing, since an enhancement in the number of E/S0s relative to late-types in small-scale, high density regions such as clusters contributes to an enhancement in their relative pair counts on all scales.

5 REAL-SPACE CLUSTERING

The radial velocities are a combination of the Hubble flow and peculiar motions. The effect of gravitational peculiar motions on small scales is to smear out high-density regions such as clusters along the radial line-of-sight. On large scales a contraction is expected due to infall into high-density regions. This gives rise to the well-known (r_p, π) -diagrams (e.g. Fisher et al. 1994, Marzke et al. 1995). In this section we determine the real-space correlation function, $\xi(r)$, in order to assess the effect of peculiar motions on the results shown in section 4. We essentially follow the prescriptions of Davis & Peebles (1983). In brief, we determine the two dimensional correlation function $\xi(r_p, \pi)$, where r_p is the separation perpendicular to the line of sight, and π is the separation along the line of sight. Only pairs separated by less than 50° in the sky and $50h^{-1}$ Mpc in space were included. As in $\xi(s)$, we adopted the Hamilton estimator and no selection effects were applied to the random catalogue.

Given $\xi(r_p, \pi)$ one may obtain the projected function $w(r_p)$ by integrating $\xi(r_p, \pi)$ along the π -direction. Once $w(r_p)$ is found one may determine the full $\xi(r)$ by solving the Abel integral

$$\xi(r) = -\frac{1}{\pi} \int_r^\infty \frac{dw(r_p)}{dr_p} (r_p^2 - r^2)^{-1/2} dr_p \quad (7)$$

numerically. In Figure 13 we show our determination of $\xi(r)$ for the ORSd and ORSm limited at 4000 km s^{-1} (panel a) and 8000 km s^{-1} (panel b), and compare it to $\xi(s)$. We use $r^2\xi(r)$ since this is a less variable quantity with scale of separation. A number of interesting features are present in this plot. First, it confirms our results based on redshift space: ORSm is more clustered than ORSd for $V_{max} = 4000 \text{ km s}^{-1}$. As before, this is not the case for the samples limited at $V_{max} = 8000 \text{ km s}^{-1}$. Thus, the results shown in section 4.2 are not an artificiality produced by redshift distortions. Figure 13 also shows that there are significant differences between $\xi(r)$ and $\xi(s)$ in all samples: $\xi(r)$ is larger than $\xi(s)$ on small scales, as expected. On large scales, linear perturbation theory gives a proportionality between $\xi(s)$ and $\xi(r)$, with the proportionality constant a function of $\beta \equiv \Omega_0^{0.6}/b$ (Kaiser 1987). The determination of β from ORS is beyond the scope of this paper, and will be presented in a future study.

Finally, we fitted a power law to $\xi(r)$. We derive $4.9 \leq r_0 \leq 7.3$ and $1.5 \leq \gamma_r \leq 1.7$ for the samples shown in Fig. 13. The best fit values for those cut at $V_{max} = 8000 \text{ km s}^{-1}$ are listed in Table 1.

6 CONCLUSIONS

Our conclusions are

(i) There are significant variations in $\xi(s)$ among the ORS subsamples limited in velocity at $V_{max} = 4000 \text{ km s}^{-1}$. The subsamples limited at $V_{max} = 8000 \text{ km s}^{-1}$, on the other hand, yield very similar clustering patterns, except for the ESGC. This suggests that ESOd, UGCd, ESOM and UGCm are close approximations to a fair samples, at least for the purpose of estimating $\xi(s)$ for $s \lesssim 20h^{-1}$ Mpc. This is further demonstrated by the very nice agreement found between $\xi(s)$ as determined here and those obtained from pre-

vious optical surveys covering different volumes (Davis & Peebles 1983, de Lapparent et al. 1988, Maurogordato et al. 1992, Loveday et al. 1995). We thus estimate that a sampling volume of $\sim (75h^{-1}\text{Mpc})^3$ is enough to represent the low-order clustering properties of the ensemble.

(ii) We have investigated the clustering properties of galaxies as a function of selection criteria and concluded that significant differences in $\xi(s)$ arise between diameter-limited and magnitude-limited samples only for small and local volumes, where diameter-limited samples contain a larger fraction of low-luminosity, late-type galaxies. For larger volumes, both samples are dominated by more luminous, earlier-type objects, reducing the discrepancy in $\xi(s)$. These results are largely in agreement with Zucca et al. (1991), who used smaller samples.

(iii) We confirm the existence of morphological segregation out to scales of $\sim 10h^{-1}$ Mpc as previously found by other authors (Lahav & Saslaw 1992, Mo et al. 1992, Dominguez-Tenreiro et al. 1994, Loveday et al. 1995). Early-type galaxies ($-5 \leq T \leq 0$) are more strongly clustered than late-types ($T \geq 5$), whereas Sa/Sb galaxies form an intermediate group. The difference in clustering amplitudes between E/S0s and Late-types suggests that the relative bias factor between these two morphological types is weakly dependent on scale. Our results indicate that $b_{Early}/b_{Late} \sim 1.5$ on small scales, showing a declining trend towards $b_{Early}/b_{Late} \sim 1$ on larger scales ($s \sim 10h^{-1}$ Mpc). Excluding clusters from the morphological samples does not change the overall picture; segregation is still present out to $s \sim 10h^{-1}$ Mpc and the apparent scale dependence of the relative bias factor remains. If real, this scale-dependence is in contradiction with the popular ‘linear local biasing’ prescription, in which b_{Early} and b_{Late} are constants. It would also disagree with the linear limit of the biasing scheme proposed by Kaiser (1984). Such a scale dependence may be explained if we allow for non-linear biasing, e.g. by having a higher fraction of early-types formed in high-density regions.

(iv) We compute the correlation function $\xi(r_p, \pi)$ and from it, find $\xi(r)$, the real space correlation function. This experiment confirms our previous findings in redshift space: ORSm galaxies are more clustered than those in ORSd within $V_{max} = 4000 \text{ km s}^{-1}$ but not within $V_{max} = 8000 \text{ km s}^{-1}$. $\xi(s)$ is also shallower and of smaller amplitude than $\xi(r)$ on small scales, as expected.

(v) Our qualitative results are insensitive to the particular kind of estimator used in deriving $\xi(s)$ and to corrections for peculiar velocities. They are also robust to uncertainties in the selection functions derived for ORS or to the particular weighting scheme used to compensate for selection effects or to combine the different subsamples.

An interesting question is whether the results found in this work hold when higher order clustering statistics are used. These latter are also important as means of testing scale-invariance relations (Bouchet et al. 1993). The determination of counts in cells and high order correlations is in progress and will be shown in a forthcoming paper (Hermit et al. 1996, in preparation).

6.1 Acknowledgements

This work was carried out at the Institute of Astronomy, Cambridge University. SH also acknowledges support from

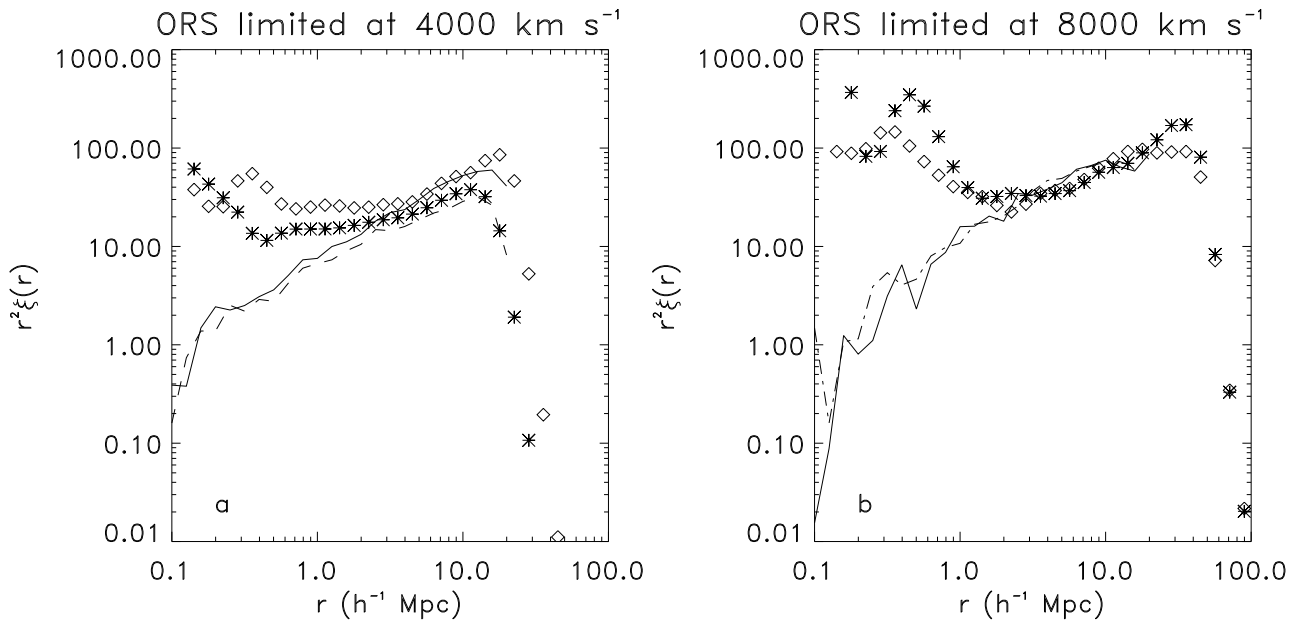


Figure 13. The real space correlation function $r^2\xi(r)$ plotted against separation r for the ORSd (stars) and ORSm (diamonds) limited at 4000 km s^{-1} (panel a) and 8000 km s^{-1} (panel b). Shown is also the redshift space correlation function, $s^2\xi(s)$ for ORSd (dashed line) and ORSm (solid line).

Julie Marie Vinter Hansens Rejselegat, Det Naturvidenskabelige Fakultet and Det Internationale Kontor at Copenhagen University. SH would like to thank Lars L. Christensen for stimulating discussions. MAS acknowledges the support of the Alfred P. Sloan Foundation.

REFERENCES

- Abell G. O., 1965, *Ann. Rev. Astron. Astroph.*, 3, 1
 Alimi J.-M., Valls-Gabaud D., Blanchard A., 1988, *A&A*, 206, L11
 Babul A., White S. D. M., 1991, *MNRAS*, 253, 31p
 Barrow J. D., Bhavsar S. P., Sonoda D. H., 1984, *MNRAS*, 210, 19p
 Binggeli B., Sandage A., Tammann G. A., 1988, *Ann. Rev. Astron. Astroph.*, 26, 509
 Bouchet F. R., Strauss M. A., Davis M., Fisher K.B., Yahil A., Huchra J.P., 1993, *ApJ*, 417, 36
 Burstein D. & Heiles C., 1982, *AJ*, 87, 1165
 Corwin H. G. & Skiff B. A., 1994, in preparation
 da Costa L. N., Vogeley M. S., Geller M. J., Huchra J. P., Park C., 1994, *ApJ*, 437, L1
 Dalton G. B., Croft R. A. C., Efstathiou G., Sutherland W. J., Maddox S. J., 1994, *MNRAS*, 271, L47
 Davis M. & Djorgovski S., 1985, *ApJ*, 299, 15
 Davis M. & Geller M.J., 1976, *ApJ*, 208, 13
 Davis M. & Huchra J., 1982, *ApJ*, 254, 437
 Davis M., Huchra J., Latham D., Tonry D., 1982, *ApJ*, 253, 423
 Davis M., Meiksin A., Strauss M. A., da Costa N. L., Yahil A., 1988, *ApJ*, 333, L9
 Davis M. & Peebles P. J. E., 1983, *ApJ*, 267, 465
 Dekel A. & Rees M. J., 1987, *Nature*, 326, 455
 de Lapparent V., Geller M. J., Huchra J. P., 1986, *ApJ*, 302, L1
 de Lapparent V., Geller M. J., Huchra J. P., 1988, *ApJ*, 332, 44
 Domínguez-Tenreiro R., Campos A., Gómez-Flechoso M. A., Yepes G., 1994, *ApJ*, 424, L73
 Dressler A., 1980, *ApJ.*, 236, 351
 Eder J. A., Schombert J. M., Dekel A., Oemler A., 1989, *ApJ*, 340, 29
 Efstathiou G., 1988, in Lawrence A., ed., *Proc. Third IRAS Conf., Comets to Cosmology*. Springer-Verlag, Berlin, p.312
 Efstathiou G., Sutherland W. J., Maddox S. J., 1990, *MNRAS*, 247, P10
 Ferguson H. C. & Sandage A., 1991, *AJ*, 101, 765
 Fisher K. B., Davis M., Strauss M. A., Yahil A., Huchra J. P., 1993, *ApJ*, 402, 42
 Fisher K. B., Davis M., Strauss M. A., Yahil A., Huchra J. P., 1994, *MNRAS*, 266, 50
 Fisher K. B., Huchra J. P., Strauss M. A., Davis M., Yahil A., Schlegel D., 1995a, *ApJS*, 100, 69
 Fisher K. B., Lahav O., Hoffman Y., Lynden-Bell D., Zaroubi S., 1995b, *MNRAS*, 272, 885
 Geller M. J. & Huchra J.P., 1988, *ApJ*, 332, 44
 Giovanelli R., Haynes M. P., Chincarini G., 1986, *ApJ*, 300, 77
 Hamilton A. J. S., 1988, *ApJ*, 331, L59
 Hamilton A. J. S., 1993, *ApJ*, 417, 19
 Hermit S. et al., 1996, in preparation
 Hubble E. & Humason M. L., 1931, *ApJ*, 74, 43
 Huchra J., Davis M., Latham D.W., Tonry J., 1983, *ApJS*, 52, 89
 Hudson M. J., 1993, *MNRAS*, 265, 43
 Iovino A., Giovanelli R., Haynes M., Chincarini G., Guzzo L., 1993, *MNRAS*, 265, 21
 Kaiser N., 1984, *ApJ*, 284, L49
 Kaiser N., 1987, *MNRAS*, 227, 1
 Kirshner R. P., Oemler A., Jr., Schechter P. L., Sheckman S. A., 1981, *ApJ*, 248, 57
 Lahav O. & Saslaw W C., 1992, *ApJ*, 396, 30
 Lahav O., Nemiroff R. J., Piran T., 1990, *ApJ*, 350, 119
 Lauberts A., 1982, *The ESO-Uppsala Survey of the ESO(B) Atlas* (München: European Southern Obs.)
 Lauberts A. & Valentijn E., 1989, *The Surface Photometry Catalogue of the ESO-Uppsala Galaxies* (München: European Southern Obs.)
 Ling E. N., Frenk C. S., Barrow J. D., 1986, *MNRAS*, 223, 21p

- Loveday J., Peterson B. A., Efstathiou G., Maddox S. J., 1992, ApJ, 390, 338
- Loveday J., Maddox S. J., Efstathiou G., Peterson B. A., ApJ, 1995, 442, 457
- Martínez V. J. & Coles P., 1994, ApJ, 437, 550
- Marzke R. O., Geller M.J., Da Costa L. N., Huchra J.P., 1995, AJ, 110, 477
- Maurogordato S., Schaeffer R., da Costa L. N., 1992, ApJ, 390, 17
- Mo H. J. & Börner G., 1990, A&A, 238, 3
- Mo H. J. & Lahav O., 1993, MNRAS, 261, 895
- Mo H. J., Jing Y. P., Börner G., 1992, ApJ, 392, 452
- Moore B., Frenk C. S., Efstathiou G., Saunders W., 1994, MNRAS, 269, 742
- Nilson P., 1973, Uppsala General Catalogue of Galaxies, Uppsala Astron. Obs. Ann., 6
- Oort J. H., 1983, Ann. Rev. Astron. Astroph., 21, 373
- Park C., Vogeley M. S., Geller M. J., Huchra J. P., 1994, ApJ, 431, 569
- Peebles P. J. E., 1980, The Large-Scale Structure of the Universe, Princeton University Press, Princeton, New Jersey
- Pellegrini P. S., Wilmer C., da Costa L. N., Santiago B. X., 1989, ApJ, 350, 95
- Phillipps S. & Shanks T., 1987, MNRAS, 229, 621
- Postman M. & Geller M., 1984, ApJ, 281, 95
- Rowan-Robinson M., Saunders W., Lawrence A., Leech K. L., 1991, MNRAS, 253, 485
- Salzer J. J., Aldering G. S., Bothun G. D., Mazzarella J. M. Lonsdale C. J., 1988, AJ, 96, 1511
- Salzer J. J., Hanson M. M., Gavazzi G., 1990, ApJ, 353, 39
- Santiago B. X. & da Costa L. N., 1990, ApJ, 362, 386
- Santiago, B. & Strauss, M. A., 1992, ApJ, 387, 9
- Santiago, B. X., Strauss, M. A., Lahav, O., Davis, M., Dressler, A., Huchra, J. P., 1995, ApJ, 446, 457 (Paper I)
- Santiago, B. X., Strauss, M. A., Lahav, O., Davis, M., Dressler, A., Huchra, J. P., 1996, ApJ, 461, 385 (Paper II)
- Saunders W., Frenk C., Rowan-Robinson M., Efstathiou G., Lawrence A., Kaiser N., Ellis R., Crawford J., Xia X.-Y., Parry I., 1991, Nature, 349, 32
- Scharf C., Hoffman Y., Lahav O., Lynden-Bell D., 1992, MNRAS 256, 229
- Strauss M. A., Davis M., Yahil A., Huchra J., 1992, ApJ, 385, 421
- Strauss M. A. & Willick J. A., 1995, Phys. Rep., 261, 271
- Thuan T. X., Alimi J.-M., Gott J. R., Schneider S. E., 1991, ApJ, 370, 25
- Totsuji H. & Kihara T., 1969, PASJ, 21, 221
- Vogeley M. S., Park C., Geller M. J., Huchra J. P., 1992, ApJ, 195, L5
- White S. D. M., Tully R. B., Davis M., 1988, ApJ, 333, L45
- Whitmore B. C., Gilmore D. M., Jones C., 1993, ApJ, 407, 489
- Yahil A., Strauss M. A., Davis M., Huchra J. P., 1991, ApJ, 372, 380
- Zucca E., Bardelli S., Cappi A., Moscardini L., 1991, MNRAS, 253, 401